Decay kinetics of the ultraviolet and visible luminescences emitted by electron-irradiated crystalline H_2O ice[a]

S. M. Trotman
School of Mathematical and Physical Sciences, Murdoch University, Murdoch, Western Australia, 6150, Australia

T. I. Quickenden[b]
Department of Physical and Inorganic Chemistry, University of Western Australia, Nedlands, Western Australia, 6009, Australia

D. F. Sangster
CSIRO, Division of Chemical Physics, Lucas Heights Research Laboratories, Private Mail Bag 7, Sutherland, New South Wales, 2232, Australia

(Received 16 October 1985; accepted 28 April 1986)

Electron pulse irradiated samples of high purity, crystalline H_2O ice at 88 K showed three kinetically distinguishable regions of luminescence emission at 280–340 nm (band I); 320–600 nm (band II); and 450–600 nm (band III). Band II emission was assigned to the $A\,^2\Sigma^+ \rightarrow X\,^2\Pi$ transition of OH, the gas phase peak being shifted from 306.4 to ~385 nm by the ice lattice. The decay half-life of the band II emission resulting from a single, ~0.05 Mrad electron pulse, was 25 ± 3 ns and increased steeply to 210 ± 10 ns for the second pulse and then steadily decreased to 140 ± 10 ns after 20 pulses. Band II emission from the second or later pulses was resolved into a short lived component with a decay half-life of ~30 ns and a longer lived component with a half-life of ~400 ns. The latter decay fitted a second order homogeneous rate equation in which the initial concentrations of the two reactants were in the ratio $(2.6 \pm 0.1):1$ and was attributed to the formation of excited OH by electron–ion recombination in the bulk ice. The short lived band II emission was also attributed to excited OH and probably arose from a mixture of a fast intraspur recombination reaction with some other process of different reaction order. Dose accumulation (memory) effects were attributed to the accumulation of OH radicals and lattice vacancies in the irradiated ice. The band III emission had a half-life of 25 ± 5 ns and its decay kinetics were consistent with emission from species such as excited OH^- or H_3O produced when electrons tunnel from a trapping site to a geminate partner.

I. INTRODUCTION

We have previously reported[1,2] the spectral distributions and radiolytic yields of the luminescences produced between 200 and 600 nm by the radiolysis of high purity H_2O ice with 0.5 MeV electrons at 88 K. Three distinguishable regions of emission were reported, the dominant feature being a broad 320–600 nm band which peaked at 385 nm and the minor features being overlapping weaker emissions in the 280–340 and 450–600 nm regions. These observations were in general accord with the aggregate of the somewhat fragmentary results obtained by earlier workers.[3–9]

The available spectral assignments of the various ice luminescences are very tentative indeed and have been reviewed elsewhere.[1] In brief, the emission around 280 nm has been attributed[6,10] to the $A\,^2\Sigma^+ \rightarrow X\,^2\Pi$ transition of OH and the sources of the 320–600 and 450–600 nm bands are largely speculative. A notable feature of the 320–600 nm band is its dependence[1,2,4,7,9] upon accumulated dose. The emission intensity increases with each successive irradiation pulse, approaching a plateau after 25–30 pulses[1] (1.2–1.5 Mrad).

The absence of detailed kinetic studies of the various ice luminescences has greatly hindered the identification of the emitting species and the analysis of models which may explain the accumulated dose dependence of the major band. This present paper consequently describes a study of the decay kinetics of the radiolytically excited luminescences from low temperature ice. The following sections review the available kinetic studies of transient species in low temperature ice.

A. Time resolved emission studies

Only two previous investigations[7,9] of ice luminescence have included any information about the decay kinetics of the emitted light. Steen and Holteng[7] used a mechanically chopped x-ray source to excite 534 (D_2O) and 373 nm (D_2O and H_2O) luminescence from low temperature ice and found a lifetime of $\sim 10^{-4}$ s for the latter and an upper limit of 5×10^{-5} s for the former. Buxton *et al.*[9] carried out a kinetic study on the decay of the luminescence excited in pulse irradiated D_2O ice and observed emission peaks at 370 and 530 nm. They were unable to find any correlation between the decay of emission at 407 nm and the decays of the absorptions at either 600 or 2350 nm, the latter two wavelengths being the regions of the well known e^-_{vis} and e^-_{IR} absorption bands.

[a] Work carried out at the Lucas Heights Research Laboratories with assistance from the Australian Institute of Nuclear Science and Engineering.
[b] To whom reprint requests should be addressed.

 0021-9606/86/172555-14$02.10

B. Time resolved absorption studies

The literature on the time dependence of optical absorption in irradiated ice is extensive, but is complicated by the large number of variables which can affect the yields and decay characteristics of the radiolysis products. Differences in sample composition, nature of the incident radiation, dose rate, total dose absorbed, temperature, and analysis time can all cause differences in results which must be taken into account when different studies are compared. Kinetic parameters can be very dependent on the above variables, particularly if second or higher order processes are involved, and it is therefore not surprising that the reported lifetimes of transient species in ice vary greatly from worker to worker.

In order to simplify the analysis of the existing absorption literature, attention will be confined to species which absorb at temperatures near 77 K in crystalline ice, as these were the experimental conditions used in our current ice luminescence studies. Kinetic studies under these conditions have been largely restricted to the two trapped electron species, e^-_{vis} and e^-_{IR}, with little work being carried out on other major absorbing species such as OH or HO_2.

1. The e^-_{vis} trapped electron

The most commonly studied[9,11–23] absorption band in low temperature ice is that produced by the e^-_{vis} trapped electron. The band is broad and unsymmetrical, rising steeply to a peak around 630–650 nm and falling slowly towards 400 nm on the short wavelength side.

Both transient and stable components of this band have been identified,[9,11–13,16,17] the transient component decaying with a half-life[12,13] of 8–25 ns in H_2O ice near 77 K. The initial yield of transient[12,13] e^-_{vis} (0.27–0.6 species/100 eV in H_2O ice) is much greater than that of stable[11,16,17] e^-_{vis} (10^{-4}–10^{-3} species/100 eV).

The transient species is reported[9,12,13] to decay by a non-homogeneous bimolecular process, although it is uncertain[12,13] whether diffusional or tunneling kinetics predominate. The reaction partner in the decay of e^-_{vis} is probably[12] H_3O^+, although H_2O^+ and OH have also been suggested.[9,13]

The stable component of the e^-_{vis} band remains detectable[16,21] in ice samples kept in the dark at 77 K for long time periods (i.e., several hours or more), but decays rapidly at elevated temperatures,[16] or if exposed to visible light.[16,21] The traps responsible for both the stable and transient components of the e^-_{vis} band do not appear to be fundamentally different, since their spectral characteristics do not differ.[11,16,17,21] Stable e^-_{vis} electrons are presumably electrons in normal e_{vis} traps which are prevented from undergoing the usual recombination reactions, perhaps as a result of the immobilization of their reaction partners at defects in the ice lattice. It is now generally accepted[9,21,24] that the e_{vis} trap is a lattice vacancy, with the bulk of the traps being produced during[9,21,22] the irradiation process.

2. The e^-_{IR} trapped electron

A second form of the localized electron e^-_{IR} gives rise to a broad transient absorption band which peaks[9,12,19] at ~3000 nm. It has been studied almost exclusively in D_2O ice due to the relatively high infrared transparency of D_2O, although Trudel *et al.*[13] have recently reported its formation ($G = 0.06$ species/100 eV) in H_2O ice at 73 K. It has been suggested[9] that the e_{IR} traps are natural cavities between layers of oxygen atoms in the ice lattice.

The decay of e^-_{IR} depends on the radiation dose previously absorbed by the sample. In previously unirradiated samples[9] it decays by reaction with a highly mobile, homogeneously distributed reaction partner (possibly[9] H_2O^+ or unrelaxed H_3O^+). At high accumulated dose the initial decay is more rapid, and has tentatively been ascribed[9] to a geminate tunneling reaction.

C. Kinetic models in low temperature ices

There is an extensive literature[9,11–13,18,25–34] dealing with the decay kinetics of emissions from aqueous glasses and of absorptions in glasses and crystalline ice. Spectral transients in these systems are reported to decay according to a variety of rate laws, including those for first order decay, those for second order decay of homogeneously distributed species in which the reactant concentrations may or may not be equal, and those for the bimolecular recombination of heterogeneously distributed species by either tunneling or diffusion.

The existing kinetic treatments of data from spectroscopic studies of ice and aqueous glasses can be criticized on several grounds. Many workers[12,13,18,25,31,33] report conformation to a particular model, but do not report the number or nature of other models (if any) tested against the data. It is also unfortunate that the standard criteria used to establish goodness of fit are not commonly presented[9,11,13,17,25,27,31,35] when one kinetic equation is adopted instead of another.

The occurrence of second order processes in irradiated ices severely complicates comparisons between the results of different workers. Thus, although decay half-lives are common descriptors[9,12,13,21–23,36] of second order processes in irradiated ice, they depend both on the radiation dose and on the time of measurement and these usually differ from one study to another. In emission studies, a further limitation occurs because it is not possible to extract absolute values for the second order rate constant from decay data unless the quantum efficiency of photon emission is known. Such information is usually unavailable. Further problems of a statistical nature can also be generated by second order processes. Thus, variations in radiation dose from one replicate experiment to another will lead to second order decay curves which differ in shape and which, strictly speaking, should therefore not be averaged if the precise functional form of the decay is to be preserved.

In view of the above comments, it is not surprising that considerable differences in the interpretation of decay kinetics in low temperature ice exist in the literature.[11–13,18,25] The present paper directs its attention to the largely neglected area of emission decay kinetics in low temperature ice, but necessarily draws on some of the absorption kinetic studies in order to facilitate the interpretation of experimental results.

II. EXPERIMENTAL

A. Equipment and procedures

The irradiation source was a Febetron 706 pulsed electron accelerator[10a] which produced 0.53 MeV pulses of electrons, each being approximately triangular in shape and having a duration of 3 ns (full width at half-maximum). The irradiated ice was approximately cylindrical in shape with a diameter of 2.0 cm and a length of 10.0 cm. The method used to grow the ice samples from high purity water has been described previously.[1] The ice sample was mounted in an evacuated irradiation chamber and the light emitted from an irradiated area of 2.5 cm^2 passed through a Spectrosil window, lenses, and a monochromator (bandpass of 10 nm unless otherwise stated), to a well-shielded RCA 1P28 photomultiplier tube. The time resolved emission was displayed on an oscilloscope screen where it was photographically recorded. The above equipment and associated procedures have been described in detail in a previous publication.[1]

All ice samples were saturated with at least 30 irradiation pulses prior to measurement, unless otherwise stated. We have previously shown[1] that under these circumstances, all luminescences in the 200–600 nm region have reached plateau levels. We will refer to ice emitting in its plateau region as "dose saturated ice" in the remainder of this paper.

The energy deposited in the irradiated section of the ice was 0.12 J $pulse^{-1}$, but when the effect of dose per pulse on luminescence intensity was studied, the dose was reduced by factors of 0.57 and 0.35 by inserting perforated stainless steel disks between the electron accelerator and the irradiation cell. The perforated disks were calibrated calorimetrically by measuring[1] the temperature rise in a small (0.9 cm^2) aluminum target temporarily inserted in the irradiation cell in place of the ice.

B. Data analysis

The oscilloscope traces of luminescence intensity vs time were recorded permanently on 3000 ASA Polaroid film. The first 10 to 15 ns of the emission trace contained an intense peak due to the effect of Cerenkov emission on the detection system. This peak was avoided by commencing digitization of the luminescence decay 20 ns after the start of the excitation pulse. The luminescence decay often extended for a period of up to 2 μs and was manually digitized into 35 to 60 points which usually covered 3 to 4 decay half-lives.

The digitized records of luminescence intensity versus time were transferred to a PDP 10 computer for processing. The signal to noise ratios in preliminary analyses were improved by constructing at each wavelength, single composite decay curves from the mean of a number (usually 8) of replicate decays, after standardization of the areas under the separate curves. Randomly phased ripple in the decay curves was significantly reduced by this procedure. In the 280–300 nm spectral region, the weak luminescence signal (50 mV) was of similar magnitude to the ripple and therefore precise determination of emission half-lives in this region was difficult, even after the application of the above averaging procedures.

As in previous work[1] all random errors are quoted at the 50% confidence level, unless otherwise stated.

III. RESULTS AND DISCUSSION

A. Emission half-lives in dose saturated ice

Although the decay half-life has only limited value for comparing the results of different workers when second order processes are present (see Sec. I C) it is nevertheless a useful parameter for distinguishing different kinetic regions in a single study of a complex decay system. In the present work, decay half-lives have been measured at selected wavelengths between 280 and 600 nm using mean emission decay curves obtained by averaging eight replicate decays at any given wavelength.

The first, second, and third half-lives of the luminescences from high purity ice at 88 K are plotted against wavelength in Fig. 1. These half-lives are hereafter designated τ_1, τ_2, and τ_3 and are the respective times taken for the emission intensity to fall from 100% to 50%, then from 50% to 25%, and finally from 25% to 12.5% of its value at 20 ns. Figure 1 also contains for comparison purposes, the distribution of

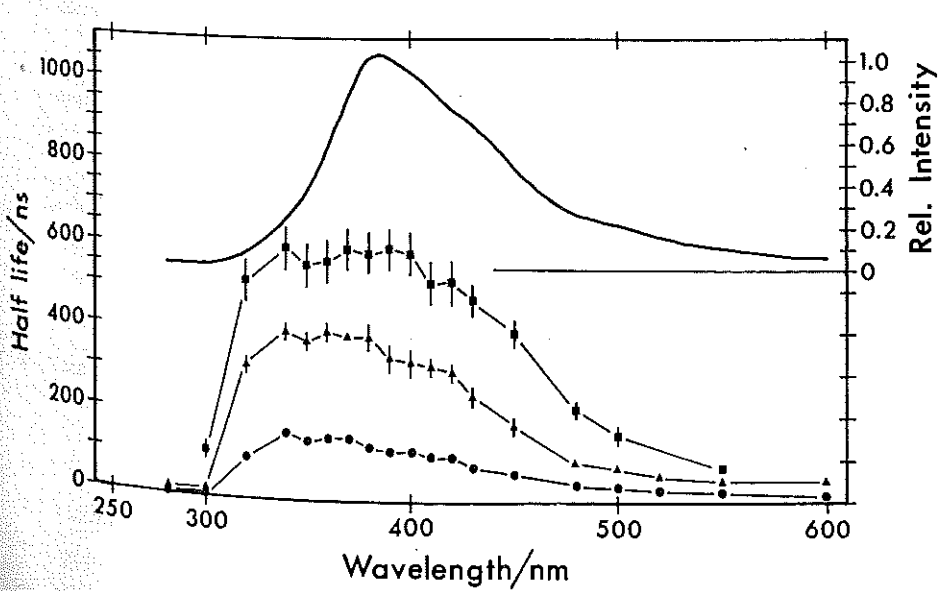

FIG. 1. The spectral distributions of the first (●), second (▲), and third (■) decay half-lives, and the luminescence intensity (—), for dose saturated, electron irradiated H_2O ice at 88 K. The half-lives were determined from the mean emission decay curves obtained by averaging eight replicate decays at each wavelength. The error bars represent 50% confidence intervals.

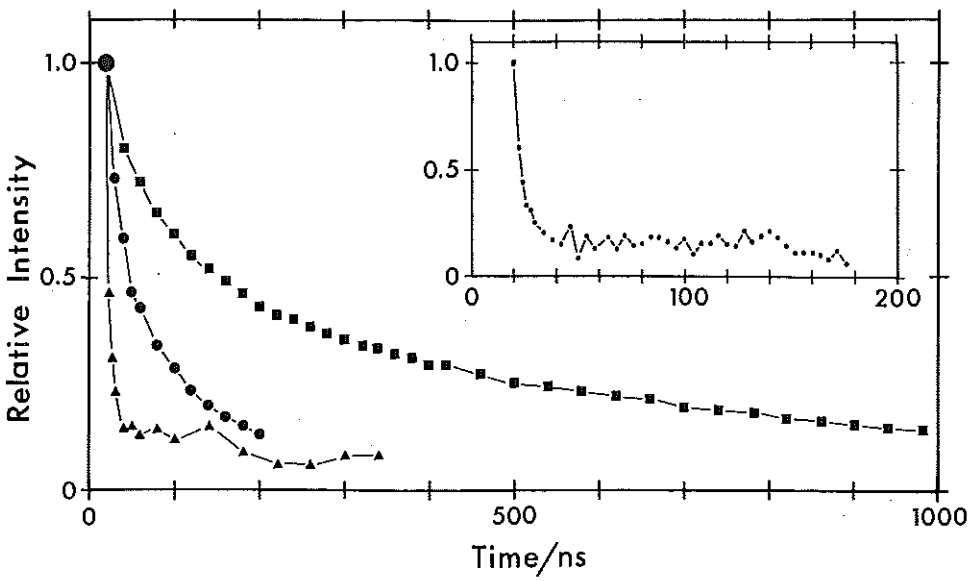

FIG. 2. Representative decay curves from the three luminescence bands excited by electrons in dose saturated H_2O ice at 88 K. Mean decay curves for 280 (▲), 380 (■), and 550 nm (●) emissions are shown. The inset shows the 280 nm decay in greater detail. All curves have been normalized to unit intensity at 20 ns. Each curve is the mean of eight replicate decays, obtained from duplicate measurements on four separate ice samples.

emission intensity with wavelength from a previous investigation.[1]

The spectral distributions of the half-lives in Fig. 1 clearly support the subdivision[2] of the ice luminescence spectrum into three distinct bands. One process leads to a short lived ($\tau_1 \simeq 4$ ns) emission between 280 and 300 nm, and a second process gives rise to a relatively long lived ($\tau_1 \simeq 130$ ns) emission between 320 and 420 nm. A third process is responsible for the emission which has an intermediate half-life ($\tau_1 \simeq 30$ ns) in the 500 to 600 nm wavelength region. These three emissions will hereafter be referred to as bands I, II, and III, respectively. The decrease in half-life between 400 and 500 nm (Fig. 1) reflects the overlap[2] of bands II and III.

Two additional points can be made about the half-lives in Fig. 1. First, each may represent the half-life of a chemical process leading to the production of excited species, or alternatively may represent the half-life for the radiative deexcitation of the excited species, depending on which of the two processes is the slower. Second, all the half-lives in Fig. 1 increase markedly with time, which indicates either that the processes are second (or higher) order, or that two or more processes with different half-lives are responsible for the emission at any one wavelength.

Figure 2 shows three decay curves representative of the three emission bands in dose saturated ice. The band I (280 nm) decay is shown in greater detail in the inset and clearly contains two components, one short lived and the other relatively long lived but much less intense. These two components may arise from the same emitting species generated in two different ways. Alternatively, the longer lived component might be due to some other species or it could be the short wavelength end of a broad band which underlies most of the spectral region investigated in this study and which emerges as the dominant component in the 500–600 nm region (band III). The latter possibility seems unlikely as the emission half-life increases steeply with wavelength as one moves from 300 to 340 nm (Fig. 1) whereas the spectral intensity rises much more slowly through this region. If a significant underlying emission with a half-life of about 30 ns had been present in this region, a slow transition from the short half-life of the band I emission to the long half-life of the band II emission would have been expected.

Unfortunately, the intensity of the tail of the 280 nm decay was too weak for the above questions to be resolved by a kinetic study of the longer lived component. Subsequent discussions of the band I luminescence will thus be limited to the early short lived component, measured at 20 ns, unless otherwise stated.

B. The dose dependence of the luminescence from dose saturated ice

The relationship between emission intensity I and the dose per pulse D in dose saturated ice was studied over a threefold variation in D. Under the conditions of dose saturation (i.e., after 25–30 pulses of ~0.05 Mrad each) the emission following each subsequent irradiation pulse of fixed dose, is of constant intensity. Varying the dose per pulse then enables one to obtain kinetic information uncomplicated by concurrent changes from the accumulated dose (memory) effect.

We will assume that the luminescence arises from a simple homogeneous recombination process (rate constant k_r) after the excitation of the ice by a short lived pulse of electrons. Thus:

$$\text{Ice} \xrightarrow{D} A_1 + A_2 + \cdots A_m$$

and

$$A_1 + A_2 + \cdots A_m \xrightarrow{k_r} C + h\nu ,$$

where the species A_i are the radiolytic products which undergo luminescent recombination to form C. The initial concentration $[A_{i,0}]$ of any species A_i, is given by

$$[A_{i,0}] = 0.01 G(A_i) D ,$$

where $G(A_i)$ is the radiolytic yield of A_i. The initial emission intensity I_0 is then

$$I_0 = \phi k_r (0.01)^m G(A_1) G(A_2) \cdots G(A_m) D^m ,$$

where ϕ is the quantum efficiency of the emission process. A plot of $\ln I_0$ against $\ln D$ should therefore be a straight line of slope m, which equals the reaction order, i.e.,

$$m = \partial(\ln I_0)/\partial(\ln D) . \quad (1)$$

Equation (1) refers to initial emission intensities, before any decay has occurred and as a result is strictly only applicable to intensities measured at the beginning of a decay generated by an infinitely narrow excitation pulse. When intensities are measured at some finite time t after excitation, it can be shown[37] that for a second order process where $[A_{1,0}] = [A_{2,0}]$:

$$\partial(\ln I)/\partial(\ln D) = 2/(1 + k_r [A_{1,0}] t) . \quad (2)$$

As t tends to zero, Eq. (2) converts to Eq. (1) with $m = 2$. However, for intensities measured at nonzero times $\partial(\ln I)/\partial(\ln D)$ is less than 2 and has a value of 1 when the intensity is measured at the first half-life. For a first order process, $\partial(\ln I)/\partial(\ln D)$ has a value of 1 for all values of t.

In order to obtain m in the present study, the intensity of the emission from dose saturated ice was measured 20 ns after the start of the excitation pulse for three different values of dose per pulse (Sec. II). The slopes of the plots of $\ln I$ vs $\ln D$ were determined by the method of weighted linear least squares and are listed for selected wavelengths in Table I. As discussed above, if non-first-order reactions are involved, these slopes will approach the reaction order only in the limit of zero time. However, as 20 ns$\ll\tau_1$ (Fig. 1) over most of the wavelength range considered, the values of $\partial(\ln I)/\partial(\ln D)$ in Table I will be reasonable approximations to the orders of the processes generating the early emissions.

Table I shows that all the reaction orders between 320 and 500 nm are significantly greater than 1 and thus indicates that there is a non-first-order component in the band II emission. The reaction orders at 550 and 600 (band III) and 280 and 300 nm (band I) do not differ significantly from 1 and thus indicate that first order processes or second order intraspur recombination reactions (which also show first order concentration dependences) are responsible for the emissions in bands I and III.

TABLE I. The dependence of light intensity I on radiolytic dose D at selected wavelengths, for dose saturated ice at 88 K. Each value of $\partial(\ln I)/\partial(\ln D)$ was obtained from a weighted linear least squares fit to a plot of $\ln I$ vs $\ln D$ for three different values of D. For each value of D, I was the mean of six replicate measurements of the emission intensity at 20 ns, three replications being carried out on one ice sample and three on another. Each error is the 50% confidence interval in the slope of the fitted line.

Wavelength/(nm)	$\partial(\ln I)/\partial(\ln D)$
600	1.09 ± 0.10
550	1.11 ± 0.14
500	1.21 ± 0.03
450	1.18 ± 0.06
420	1.28 ± 0.01
400	1.12 ± 0.08
380	1.31 ± 0.03
360	1.24 ± 0.20
340	1.26 ± 0.07
320	1.09 ± 0.04
300	1.02 ± 0.30
280	0.92 ± 0.08

C. The time dependence of the luminescence from dose saturated ice

1. Kinetic models for emission decay

Only the band II and III luminescences were intense enough to permit accurate fitting of kinetic models to the emission decays. Model fitting was carried out at 12 representative wavelengths between 320 and 600 nm. A total of five different models were tested against each individual decay curve. These models were based on: (1) first order decay; (2) homogeneous second order decay with equal reactant concentrations; (3) homogeneous second order decay with unequal reactant concentrations; (4) heterogeneous second order decay according to tunneling kinetics; and (5) heterogeneous second order decay according to diffusional kinetics.

Model 1 applies if the emission arises from the luminescence of a speciesc C* produced directly by the irradiation pulse or by a series of fast processes which culminate in a rate determining first order step. In this model, the luminescence follows a simple first order decay[38] of the form

$$I = k_f [C_0^*] e^{-k_f t} , \quad (3)$$

where I is the luminescence intensity, k_f is the rate constant for the first order emission of luminescence, t is the time, and $[C_0^*]$ is the initial concentration of the electronically excited species, C*.

Models 2 and 3 assume that the luminescent species C* is produced by the recombination of two homogeneously distributed radiolysis products, A and B, with equal and unequal concentrations, respectively. In the case of model 2:

$$I = k_r [A_0]^2/(1 + k_r [A_0] t)^2 , \quad (4)$$

where k_r is the rate constant for the recombination reaction and $[A_0]$ ($= [B_0]$) is the initial concentration of A. In the case of model 3,

$$I = k_r [A_0]^2 R e^{wt} (1 - R)^2/(R - e^{wt})^2 , \quad (5)$$

where $R = [A_0]/[B_0]$ and w is given by

$$w = k_r [A_0] (1 - R) .$$

Both Eqs. (4) and (5) can be readily obtained from the conventional[38] expressions for the rates of homogeneous second order processes.

Models 4 and 5 cover the situation in which C* is produced by the recombination of heterogeneously distributed A,B pairs which have been formed in a spur. In these cases, the luminescence decays according to[28,30]

$$I = P t^{-\beta} , \quad (6)$$

where β has a value of unity if the recombination occurs by a tunneling mechanism and where β equals 1.5 if recombination occurs via diffusion. P is a constant for a given radiation type and dose and depends upon the spatial distribution of radiation products in the spur.

The five models were tested against the experimental decay curves by fitting in turn, Eqs. (3), (4), (5), and (6) to each decay curve which comprised a set of 30 to 60 points. In

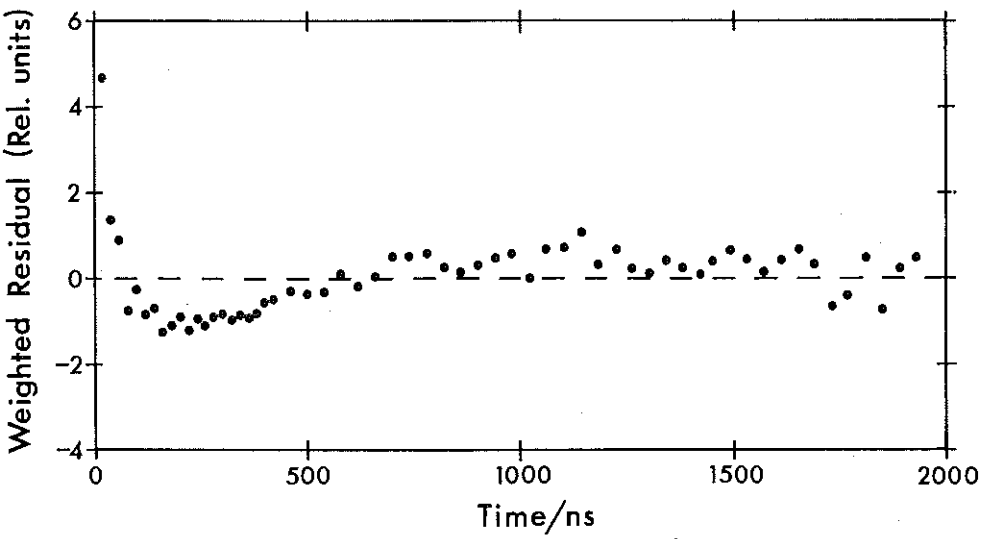

FIG. 3. A residuals plot obtained by fitting a second order rate equation (equal concentrations, model 2) to a single luminescence decay curve at 380 nm for dose saturated, irradiated H_2O ice at 88 K. The correlated residuals below 300 ns suggest that the early decay contains a short lived component which follows a decay equation different from that obtaining between 300 and 2000 ns. Each residual is defined as the difference between the measured and fitted light intensities, divided by the square root of the variance of the measured intensity.

the case of Eq. (5), concentration ratios R of 1.1, 1.2, 1.3, 1.5, 2.0, 3.0, 4.0, 6.0, 8.0, 10.0, and 12.0 were examined for optimal fit.[39] The fitting procedure for each model utilized the nonlinear, maximum likelihood techniques available in the Rothamsted MLP programming package.[40] The goodness of fit of a given model to a particular data set was determined from the weighted sum of squares of residuals SSR$(n-r)$ in conjunction with a visual inspection of a plot of the weighted residuals. The rate equation of best fit was taken to be that for which SSR$(n-r)$ was a minimum, and which also gave an essentially random[41] residuals plot. The reduced chi-square test[42] could not reasonably be applied in the present work, due to the errors introduced into a single decay by the variability of the excitation pulse and the Cerenkov induced ripple.

As many of the decay curves involved second order processes and as the electron dose from the Febetron varied slightly from sample to sample, the form of each decay curve would be expected to vary somewhat from pulse to pulse. Consequently, replicate decay curves were not generally meaned before curve fitting, but were fitted separately, the decay parameters for the replicates (usually eight) then being meaned. The only exceptions to this procedure were the curves at 550 and 600 nm, where signal to noise ratios were highest and where preliminary studies had indicated essentially first order behavior.

2. Band II emission

At all wavelengths between 320 and 550 nm inclusive, no single model would adequately fit a complete decay curve over its full time range. All models gave strongly correlated residuals plots which showed large deviations at short times. A typical example is illustrated in Fig. 3, for a model 2 fit at 380 nm. The simplest explanation for this behavior is that there are two components in the decay, one being short lived.

Decay curves at wavelengths between 320 and 450 nm, from which the early (<300 ns) points were deleted, conformed[43] consistently to a homogeneous second order rate law [model 3, Eq. (5)] with $R \simeq 2.6$. Figure 4 shows residuals plots, and sums of squares of residuals, for the curve fittings associated with Eqs. (3)–(6), over the 300 to 1980 ns portion of a single decay curve at 380 nm. All four residuals plots are to the same scale and the homogeneous second order plot with $R = 2$ [Fig. 4(C); Eq. (5)] clearly gives the best fit. Optimization of the value of R at this wavelength was carried out by fitting Eq. (5) to the data using the 11 different values of R. Figure 5 shows the corresponding residuals as a function of R and indicates that the best fit is obtained when R is about 2.3. In order to determine the sensitivity of the fitting procedure to the choice of the time

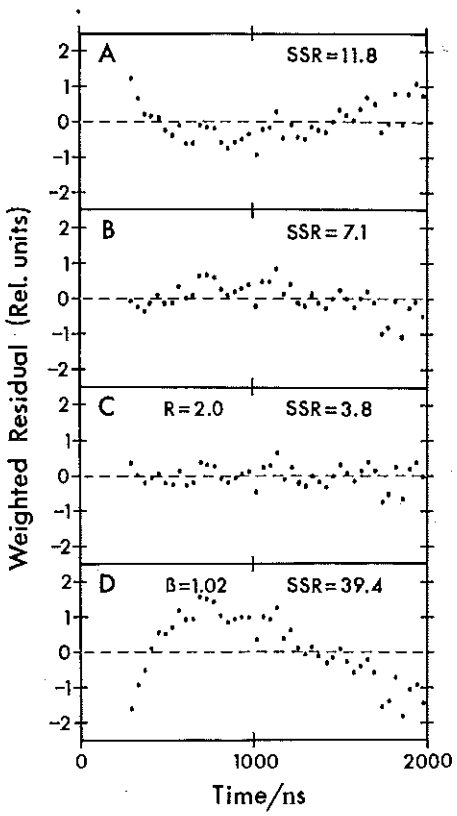

FIG. 4. Residuals plots obtained by fitting models 1–5 to the 300–1980 ns portion of the ice luminescence decay at 380 nm. Other conditions as in Fig. 3. A: first order (model 1); B: second order (equal concentrations, model 2); C: second order (concentration ratio, $R = 2.0$, model 3); D: heterogeneous second order via tunneling or diffusion (models 4 and 5, respectively). SSR is the sum of the squares of the weighted residuals.

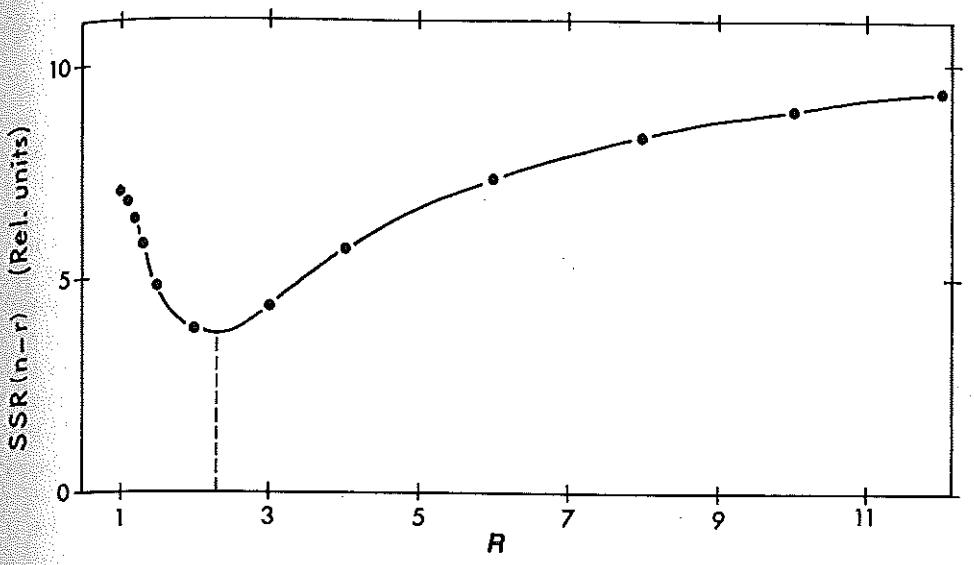

FIG. 5. The optimization of the ratio R of the concentrations of reactants in a second order (model 3) fit to the 300–1980 ns ice luminescence decay at 380 nm. The sum of squares of weighted residuals [SSR$(n-r)$] is a minimum at $R \simeq 2.3$.

origin, the above treatment was repeated on two decay curves derived from the original curve by incrementing the time coordinates of each point by -10 and -20 ns, respectively. All three curves gave virtually identical results.

Table II shows mean values of R obtained from identical analyses of the long time ($\geqslant 300$ ns) portions of eight replicate decay curves at each of the wavelengths listed. The errors were determined from the variability in the minima of the eight residuals vs R plots at each wavelength. R does not vary significantly across the 320 to 450 nm wavelength range and the weighted mean of the values therefrom is 2.6 ± 0.1.

The kinetics of the long lived component of the band II emission are characteristic of a species produced by a homogeneous interspur recombination reaction. At least some of the short lived component of the band II emission could arise from intraspur recombination of the same precursors. A lower limit to the magnitude of the short lived component at 380 nm was estimated by extrapolating Eq. (5), using the best fit value of R, to $t = 20$ ns and subtracting the extrapolated curve from the total emission decay. In each of the eight sets of replicate data, the short lived component contributed at least 40% of the total emission intensity at 20 ns, but decayed to less than one-tenth of its 20 ns value within 200 ns. The first half-lives of the short and long lived components were 30 and 400 ns, respectively.

TABLE II. Mean values $\overline{R}$ of the optimum initial concentration ratio obtained from fitting a second order equation (model 3) to the >300 ns portion of the luminescence decays from dose saturated ice, at selected wavelengths in the band II region. The errors in $\overline{R}$ have been determined at the 50% level of confidence, from the variability in the positions of the minima of the eight plots of SSR$(n-r)$ vs R (see Fig. 5) at each wavelength.

Wavelength/nm	$\overline{R}$
320	3.0 ± 0.6
340	2.6 ± 0.1
360	2.6 ± 0.05
380	2.5 ± 0.05
400	2.3 ± 0.3
420	1.8 ± 0.4
450	3.1 ± 0.9

The initial intensities of both the short and long lived components of the emission from a dose saturated sample are much larger than the initial intensity from a previously unirradiated sample (Sec. III D). The precursors of both components must therefore accumulate with repeated irradiation pulses, which further suggests that they have closely related origins. It is important to note that band III emission (mainly the 500 to 600 nm emission) does not accumulate with dose and that it can therefore be only a minor contributor to the short lived component of band II, even though this latter component and the band III emission have very similar half-lives.

Unfortunately, the uncertainties introduced by the extrapolation procedure used for separating out the short lived emission from the longer lived emission, preclude any rigorous analysis of the former. A tentative examination of the short lived emission showed that none of the rate equations associated with the five models fitted this data consistently. It is possible that other emissions besides the intraspur recombination luminescence are present in the short lived component of band II.

3. Band III emission

Figure 6 shows residuals plots derived from fitting Eqs. (3)–(6) to a mean decay curve at 600 nm. The band III emission fits Eq. (6) best, Fig. 6(D) showing the most random residuals plot and the lowest sum of square of residuals. The best fit was achieved when β of Eq. (6) had a value of 0.96, which is sufficiently close to 1 to indicate that the rate limiting step involves tunneling kinetics. Although the fit to Eq. (6) is only marginally better than that to Eq. (5), the first order dependence of the band III emission intensity upon dose (Table I) indicates that homogeneous recombination processes do not contribute strongly to the luminescence. It therefore seems likely that the band III luminescence arises from a species produced by the tunneling of an electron to a heterogeneously distributed reaction partner. The small temperature dependence of the 534 nm emission observed by Steen and Holteng[7] from D_2O ice is consistent with this assignment, as temperature independence is char-

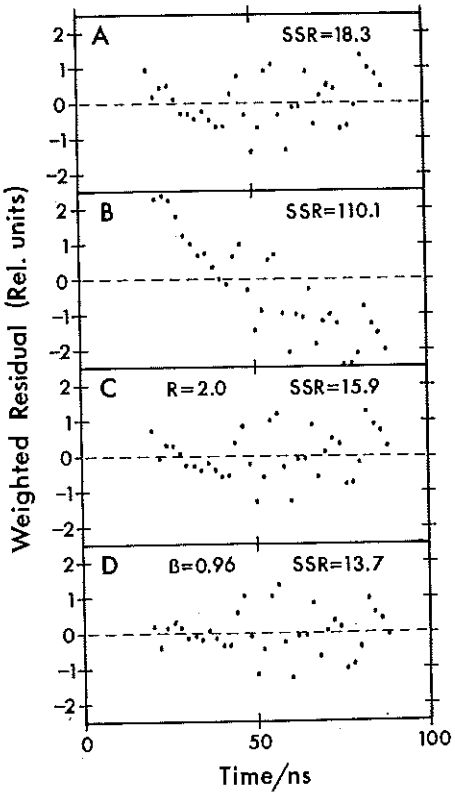

FIG. 6. Residuals plots obtained by fitting models 1–5 to the 20–88 ns portion of the ice luminescence decay at 600 nm. Other quantities as in Fig. 4.

acteristic of tunneling reactions.

The overlap of band III with band II in the 450–550 nm region is clearly evident in the emission decay curves. Thus, the long lived tail characteristic of band II (Fig. 2) is present in all the decay curves between 450 and 550 nm, but is responsible for significantly less of the total emission at longer wavelengths.

D. The effect of dose accumulation on the decay kinetics of band II

Figure 7 shows luminescence decay curves produced by the first, third, and thirtieth excitation pulses to previously unirradiated ice at 370 nm (in the band II region). The decay curve produced by the first irradiation pulse is much steeper than those produced by subsequent pulses. This difference is clearly illustrated in Fig. 8, which shows the first half-life τ_1 (the time taken for the emission intensity at 20 ns to fall by 50%) as a function of the number of excitation pulses. τ_1 increases steeply from 25 to ~230 ns between the first and third excitation pulses, but then decreases to a steady value of ~140 ns after approximately 25 pulses.

The emission decays which follow the second and subsequent irradiation pulses all follow the same basic decay pattern described in Sec. III C for the band II emission in dose saturated ice. Thus, there are two discernible components to the decays, the first being complex and short lived and which gives way after about 300 ns to a long lived tail which obeys a second order rate law (model 3). A very important feature of the long lived component is that the ratio R of the initial concentrations of reactant species does not vary significantly as the pulse number increases from 2 to its saturation value of ~30 (Fig. 9), despite a corresponding 16-fold increase[2] in the emission intensity.

This observation is not consistent with a model for the accumulated dose effect which we have proposed[1] previously on the basis of intensity data alone. However, although that model is incomplete, the proposed[1] mechanism for species accumulation can be incorporated[37] into other more comprehensive models which are consistent with the above observation.

The 370 nm emission decay which arises after the first irradiation pulse is very different from the decays which follow subsequent pulses (Fig. 7). The long lived tail which dominates the emissions from later pulses is much less in the first pulse emission, and contributes no more than about 20% of the total luminescence at $t = 20$ ns. As was the case for the short lived emission component in the dose saturated sample, the decay following the first pulse is not well described by any of the simple rate laws embodied in kinetic models 1–5.

The steep increase in emission half-life between the first and second irradiations (Fig. 8) shows that the dominant emission processes after 20 ns are different in the two cases.

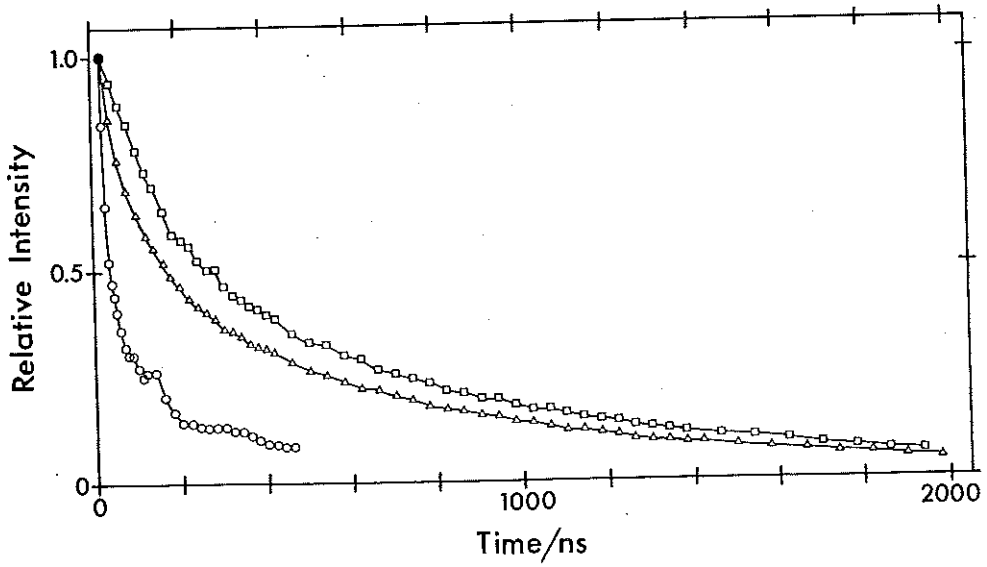

FIG. 7. The effect of dose accumulation on the decay of the 370 nm luminescence from electron irradiated ice at 88 K. Three mean decay curves are shown for the emission following the first (○), third (□), and 30th (△) excitation pulses to a previously unirradiated sample. Each curve is the mean of three replicate decays obtained from measurements on three different ice samples. The three curves have been normalized to unit intensity at 20 ns.

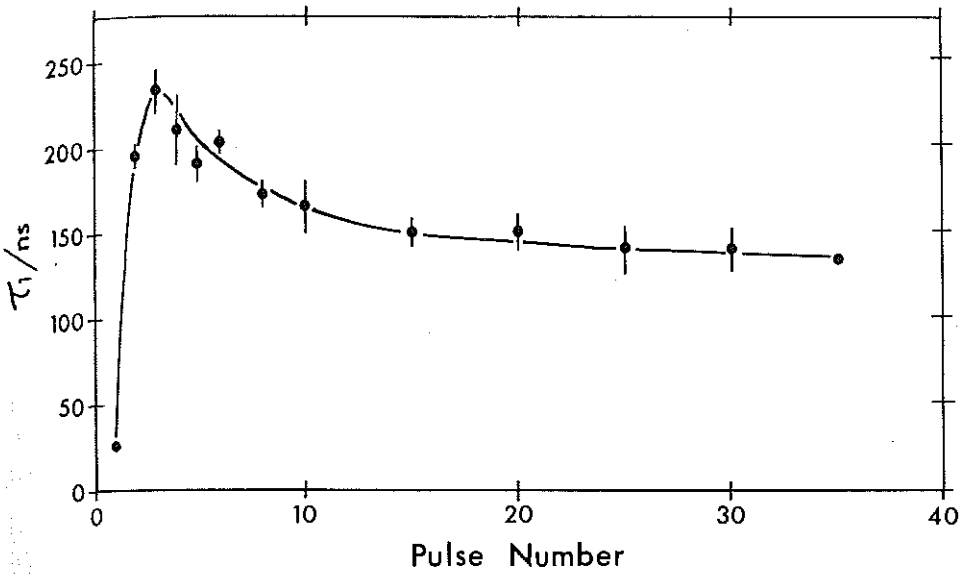

FIG. 8. The effect of electron dose accumulation on the first half-life τ_1 of the 370 nm ice luminescence at 88 K. Each error bar is the 50% confidence interval in the mean of four replicate determinations at each pulse number.

This is not unreasonable, since short lived *intraspur* reactions might be expected to predominate in ice exposed to a single excitation pulse, whereas the reactions which follow succeeding pulses would contain an additional and increasing *interspur* component due to accumulated radiolysis products. Throughout this paper, the term "spurs" is used to refer to all regions in which radiolysis products are distributed inhomogeneously, including those regions which are sometimes designated[46] as blobs and short tracks. The decrease in half-life after the third irradiation pulse would be expected from the effect of increased species concentration on the second order process which contributes to the band II emission.

E. Assignment of the emission bands

Table III summarizes the major characteristics of the three emission bands identified in this work. Species[11,12,24,36,44–67] which may be present in high purity ice in significant concentrations within a few nanoseconds of the passage of ionizing radiation include H_2O, H, OH, e^-_{vis}, e^-_{IR}, H_2, H_2O_2, HO_2, OH^-, H_3O^+, H_3O, H_2O^+, and H^-. The following sections examine which of these species are likely to be responsible for the emissions summarized in Table III and the possible processes leading to their formation. It is noted that the radiolytic photon yield for each of the three emission bands is very low[1,2] and although it is likely that the emitting species are major reaction products possessing very low quantum efficiencies for emission, it remains possible that they are products of relatively minor reactions of substances which are produced in low yield but which have high quantum yields for emission.

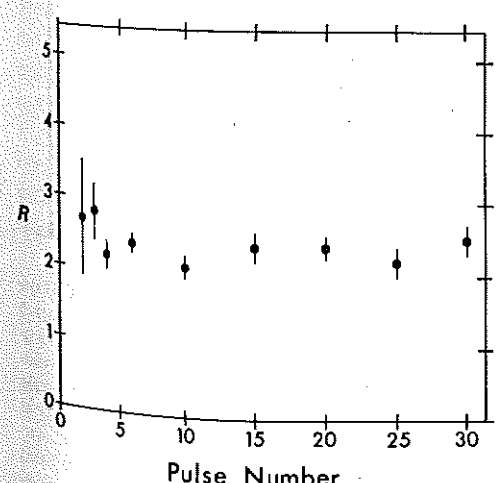

FIG. 9. The effect of dose accumulation on the optimal value of the concentration ratio R in the second order (model 3) fit to the 300–1980 ns section of the ice luminescence emitted at 370 nm. Each error bar is the 50% confidence interval in the mean of four replicate determinations of R.

1. Source of band II emission

The transition which most readily accounts for the major spectral and kinetic features of band II is the $A\,^2\Sigma^+ \rightarrow X\,^2\Pi$ transition of OH. Emission from this transition dominates the spectra obtained in numerous studies[68–81] of water vapor luminescence and has been suggested[82–85] as a source of emission in other aqueous systems. It is thus reasonable to expect that emission from $OH(A\,^2\Sigma^+)$ might be detected from irradiated ice. We disagree, however, with earlier studies[6,10] which assign this OH transition to the much weaker emission around 280 nm (band I in our work) instead of to the major 300–400 nm band. This matter is discussed further in the later section on band I emission.

H^-, H_2O_2, and H_2 can be readily eliminated as sources of the band II emission. The H^- ion possesses only one quantum state and does not produce[86] emission lines, H_2O_2 is known[4,7] to quench ice luminescence in the vicinity of 380 nm, while saturation of ice with H_2 has no effect[7] on the luminescence intensity.

Excited OH^- has been postulated as the emitter of a broad 400–500 nm band from irradiated aqueous solutions[87] and aqueous glasses,[33] but it is unlikely to be the source of the band II emission in pure ice, since the luminescence intensity appears to be unaffected[4] if samples are doped with LiOH. Furthermore, the ionization energy of OH^- is estimated[87] to be only 3.3 eV when all species are fully hydrated, in which

TABLE III. A summary of the characteristics of the three emission bands from H_2O ice at 88 K.

	Band I	Band II	Band III
Approximate wavelength[2] range(nm)	280–340	320–600	450–> 600
Peak wavelength/nm	?	385	?
Radiolytic photon yield/photons $(100\ eV)^{-1}$	2×10^{-7}	2×10^{-4} (Dose saturated sample) 1×10^{-5} (Fresh sample)	1×10^{-5}
First half-life/ns	4	140 (Dose saturated sample) 25 (Fresh sample)	30
Emission decay kinetics in dose saturated ice	1st order or intraspur recombination	Two components. One is short lived ($\tau_1\simeq30$ ns) and complex—probably a mixture of first order and intraspur recombination processes. The other ($\tau_1\simeq400$ ns) is homogeneous second order, with reactant concentrations in the ratio 2.6:1.	Intraspur recombination. Probably tunneling.
Effect of accumulated dose	None	The intensities of both components increase. Large increase in half-life between first and second pulses. Half-life relatively constant thereafter.	None

case it is unlikely to be responsible for emission from ice at wavelengths shorter than 380 nm. The band II emission reaches a peak at 385 nm, but extends to wavelengths as short as 320 nm.

The most likely of the remaining candidates can be identified by considering the effects of accumulated dose. It was suggested in Sec. III C that at least part of the short lived emission component resulted from the *intraspur* recombination of the same species which react in the bulk to produce the long lived emission. Such intraspur reactions, however, are unlikely to account for the observed increase of the short lived component's intensity with accumulated dose. The probability of an accumulated radiolysis product occurring within the volume of a newly created spur will be small, and as a result the nature and extent of spur reactions should not change significantly from pulse to pulse.

However, reexcitation of accumulated ground state molecules of the luminescent species could account for the increase in intensity of the short lived component of the luminescence with repeated pulsing. If this is the case, species which accumulate in ice at 88 K, but which are mobile at the temperature ($\sim$120 K) at which the accumulated dose effect is erased,[1,2] are favored sources of the band II emission. The H atom, the e^-_{vis} electron, and the OH and HO_2 radicals all accumulate[47,48,50] in low temperature ice, but only[47,50,88] the e^-_{vis} electron and OH become mobile at temperatures near 120 K. However, the e^-_{vis} electron is characterized by a broad absorption band which peaks at about 645 nm (Sec. I B) so this species is a most unlikely emitter of luminescence in the 380 nm region.

In contrast, a red shift of the peak emission wavelength for the $A\ ^2\Sigma^+\rightarrow X\ ^2\Pi$ transition of OH from its gas phase value[89] of 306.4 nm to about 385 nm is quite consistent with the known spectral behavior of OH in ice (Fig. 10). If it is assumed that the energy levels of OH in the open, rigid ice lattice are substantially unchanged from their gas phase values, then the shape of the well known OH absorption band[11,64,90,91] in ice is readily accounted for by a slight shift in the transition probabilities in favor of excitation to vibrationally excited levels of the $A\ ^2\Sigma^+$ state. The most important point to note from Fig. 10 is that the observation of blue-

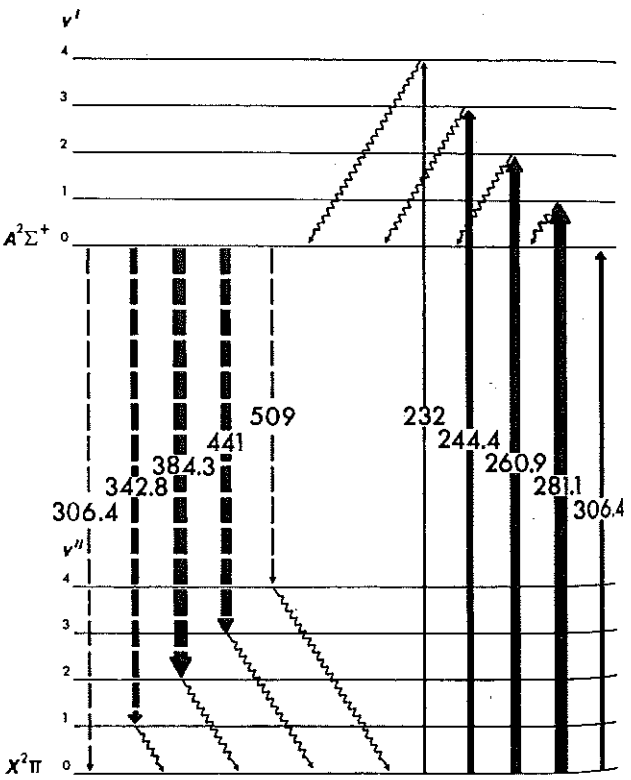

FIG. 10. A schematic representation of transitions in the $A\ ^2\Sigma^+\leftrightarrow X\ ^2\Pi$ system of OH in irradiated ice. The wavelength (in nm) corresponding to each transition is superimposed upon the appropriate vertical arrow. The "wiggly" arrows represent radiationless transitions, and it is assumed that relaxation to the ground vibrational state normally precedes electronic transition (Ref. 92). The relative strengths of the different $X\ ^2\Pi\rightarrow A\ ^2\Sigma^+$ transitions are indicated by the thicknesses of the solid vertical arrows, and are estimated from published (Refs. 11, 64, and 90) absorption spectra of irradiated ice. It is clear that emission should occur at predominantly longer wavelengths than absorption. The postulated $A\ ^2\Sigma^+\rightarrow X\ ^2\Pi$ transitions are represented by dashed arrows, and the relative transition probabilities (represented by the thicknesses of the dasbes) are estimated from the band II luminescence intensity spectrum (Ref. 2).

shifted OH absorption in ice suggests strongly that any fluorescent emission from OH* should be red shifted. Transitions from the vibrationally relaxed[92] $A\,^2\Sigma^+$ state must occur largely to vibrationally excited levels of the $X\,^2\Pi$ ground state, since the blue-shifted absorption band indicates a reduced transition probability for $A\,^2\Sigma^+(v'=0) \leftrightarrow X\,^2\Pi(v''=0)$. The emission band in the present work extends from 320 to 600 nm, and peaks at 385 nm. A shift in the Franck–Condon overlap maximum to favor the (0,2) transition is all that is required to account for the shift of this peak to 385 nm. Enhancement of the (0,1), (0,3), and (0,4) transition probabilities would readily account for the observed bandwidth. These are not unreasonable expectations, given the extensive perturbation to the Franck–Condon factors already indicated by the blue-shifted absorption band.

A further point to note from Fig. 10 is that the long wavelength limit of the absorption band should just overlap the short wavelength limit of the emission band. The long wavelength limits of the OH absorption bands reported in Refs. 11, 64, 90, and 91 are in the region of 340–350 nm, while the short wavelength limit of band II emission in the present work is about 320 nm.

If therefore appears that the most reasonable candidate for the band II emission is the excited OH radical. The radiolytic photon yield for band II is only 2×10^{-4} photons/100 eV (Table III) compared with the yield of ~ 1.2 species/100 eV for OH production,[11] but this difference is not unreasonable if quenching reactions are relatively efficient in ice. We have previously suggested[1] that OH* was an unlikely source of band II emission, based on the assumption that earlier literature assignments[6,10] of the band I emission to $OH(A\,^2\Sigma^+ \rightarrow X\,^2\Pi)$ were correct. We now believe that these earlier assignments[6,10] were incorrect.

Alternative literature assignments of emission in the band II region have been discussed in detail in an earlier publication,[1] which presents evidence against the assignment of emission to organic impurities,[93] or the recombination of electrons with alkali cations.[4] In addition, the present results do not support excited water molecules[6,8] (including the triplet exciton[8]) as a source of band II luminescence. Merkel and Hamill[6] have suggested that emission at ~ 380 nm could arise from the lowest quartet state of OH*. However, they also assigned the much weaker emission at 280 nm to $OH(A\,^2\Sigma^+ \rightarrow X\,^2\Pi)$. It is hard to understand why emission from the $A\,^2\Sigma^+$ state, which produces the dominant OH band in so many aqueous emission studies, should be so much weaker in ice compared with their proposed emission from the infrequently observed quartet state.

2. Mechanisms of band II emission

There is some evidence in the literature to suggest that electron–ion recombination plays a major role in the emission of luminescence around 380 nm. The 380 nm photoinduced luminescence reported by Bernas and Truong[10,94] was attributed by them to recombination reactions of the photodetrapped electron. Low energy excitation studies by Merkel and Hamill[6] and Prince *et al.*[8] both report a threshold for the ~ 385 nm nondelayed luminescence at around the ionization energy of water, suggesting that the H_2O^+ ion and /or the electron are precursors of much of the emission. The data presented by Prince *et al.*[8] is not conclusive, however, and it appears (Fig. 4, Ref. 8) that a minor component of the luminescence may have an excitation threshold below the ionization energy.

Steen and Holteng[7] on the other hand ruled out electron–ion recombination as a source of luminescence, since 1 mol L^{-1} concentrations of the electron scavengers CCl_3CO_2Na and $CH_2CHCONH_2$ did not affect the luminescence yields. This observation must, however, be examined in the context of the results from other dopant studies, since different workers using the same dopants have reported contradictory results,[4,7,10,95] while particular classes of dopants within a single study have had variable[7] effects. Such inconsistencies suggest that the interpretation of the results of radiolytic studies on doped ice is more complex than generally admitted.[96] Finally, it should be noted that even highly efficient electron scavenging experiments may not significantly affect the luminescence intensity if the emission arises from the recombination of mobile positive ions with trapped, rather than free, electrons.

The major features of the long lived band II emission in the present study are consistent with the bulk recombination of trapped e_{vis}^- electrons with a mobile counter ion. In particular, since empty e_{vis} sites are only one of several[90] possible reaction partners for the free electron in irradiated ice, the concentration ratio of bulk counter ions to bulk e_{vis}^- electrons would be expected to be greater than unity. This conclusion is consistent with the reactant concentration ratio of 2.6 obtained from the second order fit (Sec. III C) to the long lived band II emission decay.

Furthermore, the near absence of the long lived component of the band II emission produced by the first electron pulse to previously unirradiated ice and the growth of the long lived component with subsequent irradiations (Fig. 7) is readily explained by this model. Initially, there is only a very low concentration[9] of preexisting vacancies (empty e_{vis} traps) in the ice, but with irradiation, the number of such traps increase[9,21,22] and at least some fill with electrons and provide the trapped e_{vis}^- electrons necessary for the long lived band II emission.

Both H_2O^+ and H_3O^+ have been suggested[9,12,35,36,63,90] as the positive ion which reacts with the various forms of electron in irradiated ice. The production of $OH(A\,^2\Sigma^+)$ by electron recombination with H_2O^+ is energetically feasible, but it seems unlikely[44,63] that H_2O^+ would persist in irradiated ice for more than a few nanoseconds before it is converted to H_3O^+. Estimates of the electron affinity of H_3O^+ vary[97–101] but most lie between 3 and 5 eV. Recombination of electrons with ground state H_3O^+ is therefore unlikely on energetic grounds to generate $OH(A\,^2\Sigma^+)$. It has been suggested by Gillis *et al.*[35] that radiation produced H_3O^+ in a high vibrational energy state may be the major counterion. Unfortunately, this suggestion is difficult to test experimentally, since doping with H_3O^+ will not necessarily produce a species in the same vibrational state.

As indicated in Sec. III C uncertainties associated with the extrapolation procedure used to separate the short lived

from the long lived band II emission prevented a rigorous kinetic analysis of the short lived component. None of the rate equations (3) to (6) gave consistent fits to the short lived component of the band II emission and this probably implies a mixture of emissions of different reaction order. The same recombination reactions which produce OH in its $A\,^2\Sigma^+$ state and hence produce the long lived band II emission, can occur as either interspur or intraspur reactions. The latter would proceed at much higher rates than the former and would not exhibit the homogeneous second order kinetics observed for the interspur recombination reactions. It is therefore likely that the short lived component of the band II emission contains a substantial contribution from excited OH produced by fast intraspur recombination and a contribution from some other process of different reaction order.

The increase in intensity of the short lived band II emission with accumulated dose can be readily accounted for if the trapped OH radicals produced from pulse to pulse can be reexcited in subsequent pulses. This is not unreasonable provided there is an efficient method of energy transfer (e.g., exciton transfer) from the lattice to the trapped OH.

The loss of accumulation of both the long lived and the short lived band II emissions which occurs[1,2] when the sample is heated to about 120 K is also well accounted for by the proposed mechanisms. Trapped OH radicals become mobile[47,50,88] and rapidly react with other radiolysis products at a temperature of about 110 K. Radiation produced vacancies are destroyed[23] by annealing at 120 K. Heating the ice sample to 120 K therefore destroys the accumulated reservoirs of both OH and the e_{vis} vacancies. If accumulated OH is responsible for the increase in the intensity of the short lived emission and accumulated vacancies (which are the precursors to e^-_{vis} electrons trapped in the bulk ice) are responsible for the increase in the intensity of the long lived emission, it is not surprising that both intensity accumulations are removed by heating the ice to $\sim$120 K.

3. Band I emission

Unfortunately, the band I emission was too weak to permit a detailed study of its decay kinetics. Despite the limited experimental information available (Table III), it is still possible to eliminate many species as sources of the emission. H^- and OH^- can be eliminated for the reasons discussed in relation to band II. Merkel and Hamill[6] have reported that the threshold for the 280 nm emission is in the region of 9 eV, a value significantly below the ionization energy of H_2O. This eliminates H_2O^+ as well as its reaction products, H_3O^+ and H_3O, and suggests that electron–ion recombination will not contribute significantly to the luminescence. The trapped electron might still be generated by the excitation electrons in Merkel and Hamill's study,[6] but the trapped electron's absorption at $\sim$645 nm precludes emission at 280 nm.

H_2, H_2O_2, and HO_2 are all reported[11,47,64,88] to accumulate in irradiated low temperature ice. They are therefore unlikely to be responsible for the band I emission, which is unaffected by dose accumulation, although it remains possible that the luminescence arises from a particular excited state which is generated by a specific formation process, but is not readily reexcited in the accumulated product.

Previous assignments[6,10] for emission in this region have been restricted to the $A\,^2\Sigma^+ \rightarrow X\,^2\Pi$ transition of OH. This is the transition proposed as the source of the much more intense band II emission in the present study. The only basis for the previous assignments has been the correspondence of the 280 nm emission wavelength to the well established 280 nm OH absorption band in ice. It now seems clear, for two reasons, that the $A\,^2\Sigma^+ \rightarrow X\,^2\Pi$ transition of OH cannot be responsible for the band I emission. Firstly, as shown in Fig. 10, the blue shift of the $A\,^2\Sigma^+ \leftarrow X\,^2\Pi$ absorption peak from 306.4 nm in the vapor phase to 280 nm in ice in fact favors a red shift in the emission maximum, provided vibrational relaxation of the excited state occurs before transition to the ground state. Secondly, OH is well known to accumulate in ice at temperatures below 110 K, and yet the band I emission intensity is unaffected by dose accumulation. OH* in its $A\,^2\Sigma^+$ state is produced from H_2O under a wide variety of excitation conditions so that reexcitation of accumulated OH would be most likely to generate the $A\,^2\Sigma^+$ state. Under these conditions, the band I emission intensity would be expected to increase with accumulated dose if it originated from the $A\,^2\Sigma^+ \rightarrow X\,^2\Pi$ transition.

These arguments do not rule out the possibility that the band I luminescence arises from an excited state of OH which is less readily generated than $OH(A\,^2\Sigma^+)$ and which is produced in a fixed yield from pulse to pulse. A slight possibility remains that a specific intraspur process, which is unaffected by dose accumulation, could generate vibrationally excited $OH(A\,^2\Sigma^+)$ which is only weakly coupled to the ice lattice. Such a state might emit a photon before relaxation to the lowest vibrational level of the excited state has occurred, in which case $OH(A\,^2\Sigma^+)$ could be the source of both the band I and band II luminescences.

The most likely sources of band I emission therefore appear to be excited states of H_2O, H, or possibly OH (excluding the $A\,^2\Sigma^+ \rightarrow X\,^2\Pi$ transition), although H_2, H_2O_2 and HO_2 remain possibilities. Unfortunately a more definite assignment of the band is not possible at this time because of its very low intensity.

4. Band III emission

The intensity of the band III emission was only just sufficient to permit a study of its decay kinetics. The kinetics are most characteristic of a recombination process in which a trapped species tunnels from the trap to a geminate partner. The decays of both e^-_{vis} and e^-_{IR} have been attributed[9,13] to tunneling reactions in dose saturated ice, with the three most likely reaction partners being OH, H_3O^+, or H_2O^+, i.e.,

$$(e^-_{aq} + OH) \rightarrow OH^{-}*, \tag{7}$$

$$(e^-_{aq} + H_3O^+) \rightarrow H_3O*, \tag{8}$$

$$(e^-_{aq} + H_2O^+) \rightarrow H_2O*. \tag{9}$$

The symbol, e^-_{aq}, is used to denote either e^-_{vis} or e^-_{IR}, and the brackets indicate a nonhomogeneous recombination. The emitting species in each case is the excited recombination product, viz. OH^-*, H_3O*, or H_2O*.

Since H_2O^+ is unlikely to persist in ice for periods in

excess of a few nanoseconds, reactions (7) and (8) appear to be the most probable sources of band III emission. The corresponding reactions in the bulk medium evidently make only a minor contribution to the emission, since band III is unaffected by accumulated dose, whereas the concentrations of $e^-_{vis,bulk}$, $H_3O^+_{bulk}$, and OH_{bulk} all increase from pulse to pulse.

Previous assignments of emissions from aqueous systems in this spectral region are limited. OH^{-*} has been tentatively suggested as the emitter around 400–500 nm in irradiated aqueous solutions[87] and aqueous glasses.[33] However, at least one alternative explanation for this well known emission band has been provided by Maria and McGlynn,[85] who assign it to the $^4\Sigma^- \rightarrow X\,^2\Pi$ transition of OH.

H_3O^* has been postulated as an intermediate[44,46] in water radiolysis, but it has yet to be positively identified. It is therefore interesting to note that recent work[102,103] on the emission spectrum of H_3 suggests that excited Rydberg states of H_3O might be stable and be expected to emit in the vicinity of 550 nm.

IV. CONCLUSIONS

Kinetic studies of the luminescence from high purity, crystalline, H_2O ice irradiated at 88 K confirm[1,2] the existence of three distinct emission bands.

The intense 320–600 nm band has been assigned to the red-shifted $A\,^2\Sigma^+ \rightarrow X\,^2\Pi$ transition of OH. The decay kinetics of this luminescence suggest that several processes contribute to the production of $OH(A\,^2\Sigma^+)$, a major source being electron–ion recombination within both the spurs and the bulk ice medium. The effects of accumulated dose[1,2] on this luminescence can be at least qualitatively understood in terms of the accumulation of OH radicals and lattice vacancies in the irradiated ice.

Assignments of the two much weaker emission bands around 280–340 and 450–600 nm are more difficult, but it is possible to eliminate many water fragments from being emitters in these regions. The broad 450–600 nm band appears to originate from the intraspur reaction of trapped electrons with another species. The most likely emitters in this case are excited OH^- or H_3O. The processes leading to the very weak 280–340 nm emission are not known, but it is most unlikely that this band arises from OH in its $A\,^2\Sigma^+$ state. This latter conclusion is important in view of previous assignments[6,10] of this band to emission from the $A\,^2\Sigma^+$ state of OH.

ACKNOWLEDGMENTS

The authors wish to thank the following persons for valuable discussions during the course of this work: Dr. H. A. Gillis, National Research Council of Canada; Dr. J. A. Irvin, Photocare Limited; Dr. T. P. Speed, CSIRO Division of Mathematical Statistics; Dr. J. M. Warman, Netherlands Inter-University Reactor Institute. One of us (S. M. T.) gratefully acknowledges financial support by a Postgraduate Studentship from the Australian Institute of Nuclear Science and Engineering.

[1]T. I. Quickenden, S.M. Trotman, and D. F. Sangster, J. Chem. Phys. **77**, 3790 (1982).
[2]T. I. Quickenden, S. M. Trotman, and D. F. Sangster, Radiat. Res. **101**, 407 (1985).
[3]W. M. Jones, J. Chem. Phys. **20**, 1974 (1952).
[4]L. I. Grossweiner and M. S. Matheson, J. Chem. Phys. **22**, 1514 (1954).
[5]J. A. Ghormley, J. Chem. Phys. **24**, 1111 (1956).
[6]P. B. Merkel and W. H. Hamill, J. Chem. Phys. **54**, 1695 (1971).
[7]H. B. Steen and J. Aa. Holteng, J. Chem. Phys. **63**, 2690 (1975).
[8]R. H. Prince, G. N. Sears, and F. J. Morgan, J. Chem. Phys. **64**, 3978 (1976).
[9]G. V. Buxton, H. A. Gillis, and N. V. Klassen, Can. J. Chem. **55**, 2385 (1977).
[10]A. Bernas and T. B. Truong, Chem. Phys. Lett. **29**, 585 (1974).
[11]I. A. Taub and K. Eiben, J. Chem. Phys. **49**, 2499 (1968).
[12]K. Kawabata, Y. Nagata, S. Okaba, N. Kimura, K. Tsumori, M. Kawanishi, G. V. Buxton, and G. A. Salmon, J. Chem. Phys. **77**, 3884 (1982).
[13]G. J. Trudel, H. A. Gillis, N. V. Klassen, and G. G. Teather, Can. J. Chem. **59**, 1235 (1981).
[14]V. N. Shubin, V. A. Zhigunov, V. I. Zolotarevsky, and P. I. Dolin, Nature, **212**, 1002 (1966).
[15]K. Kawabata, S. Okabe, and S. Taniguchi, J. Chem. Phys. **57**, 2855 (1972).
[16]K. Eiben and I. A. Taub, Nature, **216**, 782 (1967).
[17]K. Kawabata, J. Chem. Phys. **55**, 3672 (1971).
[18]G. Nilsson, H. Christensen, P. Pagsberg, and S. O. Nielson, J. Phys. Chem. **76**, 1000 (1972).
[19]G. V. Buxton, H. A. Gillis, and N. V. Klassen, Chem. Phys. Lett. **32**, 533 (1975).
[20]K. Kawabata, H. Horii, and S. Okabe, Chem. Phys. Lett. **14**, 223 (1972).
[21]K. Kawabata, J. Chem. Phys. **65**, 2235 (1976).
[22]K. Kawabata, S. Okabe, and H. Horii, Chem. Phys. Lett. **20**, 586 (1973).
[23]H. Hase and K. Kawabata, J. Chem. Phys. **65**, 64 (1976).
[24]N. Riehl, B. Bullemer, and H. Engelhardt, *The Physics of Ice* (Plenum, New York, 1969).
[25]T. E. Pernikova, S. A. Kabakchi, V. N. Shubin, and P. I. Dolin, Radiat. Eff. **5**, 133 (1970).
[26]J. R. Miller, J. Chem. Phys. **56**, 5173 (1972).
[27]J. R. Miller, Chem. Phys. Lett. **22**, 180 (1973).
[28]S. J. Rzad, P. P. Infelta, J. M. Warman, and R. H. Schuler, J. Chem. Phys. **52**, 3971 (1970).
[29]F. Kieffer, C. Lapersonne-Meyer, and J. Rigaut, Int. J. Radiat. Phys. Chem. **6**, 79 (1974).
[30]M. Tachiya and A. Mozumder, Chem. Phys. Lett. **34**, 77 (1975).
[31]G. V. Buxton and K. G. Kemsley, J. Chem. Soc. Faraday Trans. 1, **71**, 568 (1975).
[32]H. A. Gillis and D. C. Walker, J. Chem. Phys. **65**, 4590 (1976).
[33]G. V. Buxton, H. A. Gillis, and N. V. Klassen, Can. J. Chem. **54**, 367 (1976).
[34]J. W. van Leeuwen, M. G. J. Heijman, H. Nauta, and G. Casteleijn, J. Chem. Phys. **73**, 1483 (1980).
[35]H. A. Gillis, G. G. Teather, and C. K. Ross, J. Phys. Chem. **84**, 1248 (1980).
[36]J. M. Warman, M. P. de Haas, and J. B. Verberne, J. Phys. Chem. **84**, 1240 (1980).
[37]S. M. Trotman, Ph.D. thesis, University of Western Australia, 1983.
[38]S. W. Benson, *The Foundations of Chemical Kinetics* (McGraw-Hill, New York, 1960).
[39]Initial attempts to fit all three unknown parameters, (k_r, $[A_0]$, and R) in Eq. (5) in a single operation were not successful. The residuals surfaces were unsymmetrical and the fits did not readily converge. A method of simultaneously fitting all three parameters was developed at a late stage of the work and applied to a representative decay curve at 380 nm. The results of the simultaneous fitting procedure agreed with those obtained by the multiple fitting procedure described in this paper.
[40]G. J. S. Ross, MLP Programming Manual (Lawes Agricultural Trust, Rothamsted Experimental Station, U. K., 1980).
[41]N. R. Draper and H. Smith, *Applied Regression Analysis* (Wiley, New York, 1966).
[42]J. A. Irvin, T. I. Quickenden, and D. F. Sangster, Rev. Sci. Instrum., **52**, 191 (1981).
[43]The emission between 450 and 550 nm also showed evidence of two component decays, but the intensities of the decay tails were too low to allow precise curve fitting at these wavelengths.
[44]I. G. Draganić and Z. D. Draganić, *The Radiation Chemistry of Water*

(Academic, New York, 1971).
[45]P. V. Hobbs, *Ice Physics* (Oxford, London, 1974).
[46]J. H. O'Donnell and D. F. Sangster, *Principles of Radiation Chemistry* (Arnold, London, 1970).
[47]L. Kevan, in *The Radiation Chemistry of Aqueous Systems*, edited by G. Stein (Weizmann Science, Jerusalem, 1968), p. 21.
[48]D. M. Brown and F. S. Dainton, Radiat. Res. Rev. **1**, 241 (1968).
[49]D. Schulte-Frohlinde and K. Vacek, Curr. Top. Radiat. Res. **5**, 39 (1969).
[50]B. G. Ershov and A. K. Pikaev, Radiat. Res. Rev. **2**, 1 (1969).
[51]E. J. Hart, Radiat. Res. Rev. **3**, 285 (1972).
[52]C. J. Hochanadel, in *Comparative Effects of Radiation*, edited by Burton, Kirby-Smith, and Magee (Wiley, New York, 1960), p. 151.
[53]H. A. Schwarz, J. Phys. Chem. **73**, 1928 (1969).
[54]W. H. Hamill, J. Phys. Chem. **73**, 1341 (1969).
[55]G. V. Buxton, Proc. R. Soc. London Ser. A **328**, 9 (1972).
[56]R. K. Wolff, J. E. Aldrich, T. L. Penner, and J. W. Hunt, J. Phys. Chem. **79**, 210 (1975).
[57]M. Kongshaug, H. B. Steen, and B. Cercek, Nature (London) Phys. Sci. **234**, 97 (1971).
[58]P. Neta, R. W. Fessenden, and R. H. Schuler, Nature (London) Phys. Sci. **237**, 46 (1972).
[59]M. Anbar and D. Meyerstein, J. Phys. Chem. **68**, 1713 (1964).
[60]R. W. Matthews, J. Chem. Soc. Faraday Trans. 1 **70**, 1384 (1974).
[61]G. V. Buxton, Radiat. Res. Rev. **1**, 209 (1968).
[62]C. D. Jonah, J. R. Miller, and M. S. Matheson, J. Phys. Chem. **81**, 1618 (1977).
[63]M. Kunst and J. M. Warman, Nature **288**, 465 (1980).
[64]J. A. Ghormley and A. C. Stewart, J. Am. Chem. Soc. **78**, 2934 (1956).
[65]T. B. Truong, Chem. Phys. Lett. **35**, 426 (1975).
[66]A. Bernas and T. B. Truong, Can. J. Chem. **55**, 2044 (1977).
[67]T. B. Truong, J. Chem. Phys. **68**, 4128 (1978).
[68]T. I. Quickenden, J. A. Irvin, and D. F. Sangster, J. Chem. Phys. **69**, 4395 (1978).
[69]I. P. Vinogradov and F. I. Vilesov, Opt. Spektrosk. **40**, 58 (1976).
[70]I. V. Shushanin and S. M. Kishko, Opt. Spectrosc. **30**, 315 (1971).
[71]P. Erman and J. Brzozowski, Phys. Lett. A **46**, 79 (1973).
[72]S. Tsurubuchi, T. Iwai, and T. Horie, J. Phys. Soc. Jpn. **36**, 537 (1974).
[73]C. I. M. Beenakker, F. J. de Heer, H. B. Krop, and G. R. Möhlmann, Chem. Phys. **6**, 445 (1974).
[74]K. D. Beyer and K. H. Welge, Z. Naturforsch. Teil A **19**, 19 (1964).
[75]C. C. Wang and L. I. Davis, J. Chem. Phys. **62**, 53 (1975).
[76]M. T. MacPherson and J. P. Simons, Chem. Phys. Lett. **51**, 261 (1977).
[77]L. C. Lee, J. Chem. Phys. **72**, 4344 (1980).
[78]M. A. A. Clyne, J. A. Coxon, D. W. Setser, and D. H. Stedman, Trans. Faraday Soc. **65**, 1177 (1969).
[79]A. C. Vikis, Chem. Phys. Lett. **33**, 506 (1975).
[80]W. R. Binns and J. L. Ahl, J. Chem. Phys. **68**, 538 (1978).
[81]G. H. Nussbaum and A. R. Cathers, J. Chem. Phys. **68**, 2521 (1978).
[82]D. N. Sitharamarao and J. F. Duncan, J. Phys. Chem. **67**, 2126 (1963).
[83]T. I. Quickenden and S. S. Que Hee, Radiat. Res. **46**, 28 (1971).
[84]K. J. Taylor and P. D. Jarman, Aust. J. Phys. **23**, 319 (1970).
[85]H. J. Maria and S. P. McGlynn, J. Chem. Phys. **52**, 3402 (1970).
[86]H. A. Bethe and E. E. Salpeter, *Quantum Mechanics of One and Two Electron Atoms* (Springer, Berlin, 1957).
[87]P. B. Merkel and W. H. Hamill, J. Chem. Phys. **55**, 2174 (1971).
[88]L. Kevan, Actions Chim. Biol. Radiat. **13**, 57 (1969).
[89]H. Mohan and Shardanand, *Free Radical OH* (N.T.I.S., Virginia, 1975).
[90]Z. Wu, H. A. Gillis, N. V. Klassen, and G. G. Teather, J. Chem. Phys. **78**, 2449 (1983).
[91]J. A. Ghormley and C. J. Hochanadel, J. Phys. Chem. **75**, 40 (1971).
[92]Vibrationally excited states would be expected to relax rapidly to the ground vibrational state in a solid.
[93]G. Vierke and J. Stauff, Ber. Bunsenges. Phys. Chem. **74**, 358 (1970).
[94]A. Bernas and T. B. Truong, C. R. Acad. Sci. Ser. B **277**, 391 (1973).
[95]J. Kaufhold and W. Kerr, in *The Thermoluminescence of Geological Materials*, edited by D. J. McDougall (Academic, New York, 1968), p. 621.
[96]A preliminary study of doped ice in the present work (Ref. 37) highlighted the effect of even small concentrations of dopants on the crystalline ice structure, suggesting that structural differences may be a major cause of apparently inconsistent results. Ice samples grown by the method described in Ref. 1, from water doped with 10^{-2}–10^{-3} mol L^{-1} $NaNO_3$, usually contained a translucent core, indicating preferential inclusion of the salt in the regions away from the irradiated surface. Rapid freezing of such samples, in an attempt to avoid segregation, produced an opaque white solid totally unlike the high purity samples in appearance. Samples grown from water containing between 10^{-1} and 1 mol L^{-1} of dopant were typically crumbly in texture and contained many small wafer-like crystals embedded in a matrix of lower melting point. It therefore seems that although the results of radiation chemical studies of doped aqueous *glasses* might be readily interpretable, it would be prudent to treat the results of similar studies on *crystalline* aqueous systems with more caution.
[97]C. E. Melton and H. W. Joy, J. Chem. Phys. **46**, 4275 (1967).
[98]K. S. E. Niblaeus, B. O. Roos, and P. E. M. Siegbahn, Chem. Phys. 25 207 (1977).
[99]R. E. Kari and I. G. Csizmadia, J. Am. Chem. Soc. **99**, 4539 (1977).
[100]B. W. Williams and R. F. Porter, J. Chem. Phys. **73**, 5598 (1980).
[101]G. I. Gellene and R. F. Porter, J. Chem. Phys. **81**, 5570 (1984).
[102]I. Dabrowski and G. Herzberg, Can. J. Phys. **58**, 1238 (1980).
[103]G. Herzberg, J. Chem. Phys. **70**, 4806 (1979).
[104]The Febetron 706 is located at the Lucas Heights Research Laboratories, New South Wales, and is operated by the Australian Institute of Nuclear Science and Engineering.